

## Sol-gel synthesis, characterization of Fe/ZrO<sub>2</sub> nanocomposites and their photodegradation activity on indigo carmine and methylene blue textile dyes

Mohammed Ahmed Wahba, Walied A. A. Mohamed\*, Adli A. Hanna

Inorganic Chemistry Department, National Research Centre, Cairo, Egypt.

**Abstract :** Pure ZrO<sub>2</sub> as well as a series of Fe/ZrO<sub>2</sub> nanocomposites with varying iron content (1, 3, 5 and 8 %) have been successfully prepared using a modified sol-gel Pechini method. Phase structures, crystallite size and morphologies were studied by X-ray diffraction and scanning electron microscope techniques. The results showed that Fe-doping have a remarkable impact on both phase structure and crystallite size. Increasing the doping percentage reduced both the average crystallite size (from 30 to 18 nm) and lattice parameters of unit cells. Photocatalytic degradation of the samples against indigo carmine and methylene blue dyes has been evaluated. Perceptible impact of the iron loading on photocatalytic activity of Zr-Fe samples was observed. Photocatalytic degradation reaction rates of methylene blue and indigo carmine enhanced upon increasing the doping percent and found to fits a first order reaction.

**Key words:** Fe/ZrO<sub>2</sub>, Sol gel, indigo carmine, methylene blue and photodegradation.

### 1.0 Introduction

Problems of water contaminations are currently up-raising challenges to human beings and environment. The majority of water problems have been always originated from industrial processes<sup>1</sup>. Sulfur, asbestos, heavy metals, nitrates, phosphates, oil and non-biodegradable dyes are the major industrial causes of water pollution<sup>2</sup>. Dye industries are representing a highly hazardous reason for this challenging problem, they involve discharging of toxic aromatic intermediates as well as chemically stable organic dyes, which resist natural degradation hence are subjected to transform into carcinogenic agents<sup>3</sup>. The problem of toxic dyes pollution can be faced effectively through two kind of process a) adsorption on a suitable substrate<sup>4,5</sup> b) degradation to nontoxic metabolites<sup>6,7</sup>. In the former method, problems of incomplete adsorption, disposal of the sludge and adsorbent recovery are the main disadvantages<sup>8</sup>. On the other hand, degradation of dyes by chemical or biological oxidation is appropriate and has been extensively explored<sup>6,7</sup>. However, new generation of dyes are manufactured to resist microbial attack and as a result conventional biological wastewater treatment is unproductive for their degradation<sup>9</sup>. To overcome this problem, an alternative trend for treatment of hazardous organic pollutants such as dyes in water is done using nanoparticles<sup>9</sup>. Photodegradation using metal oxide photocatalyst is an outstanding method for organic pollutant degradation and has proved to be as an efficient tool for degrading both atmospheric and aquatic organic contaminants. It uses the sunlight in the presence of a semiconductor photocatalyst to accelerate the remediation of environmental contaminants, destruction of highly toxic molecules and wastewater treatment<sup>10-13</sup>. TiO<sub>2</sub>, V<sub>2</sub>O<sub>5</sub>, ZnO, WO<sub>3</sub>, and ZrO<sub>2</sub> have been explored as promising photocatalysts semiconductors<sup>14,15</sup>. Mechanism of photocatalyzed dye degradation using semiconducting materials can be categorized into i) indirect photo-degradation ii) direct photo-degradation processes: The indirect photocatalytic oxidation mechanism involves: photoexcitation, ionization of water oxygen, ionosorption and protonation of superoxide<sup>16</sup>. On the other hand, the direct mechanism involves

excitation of dyes under photon of visible light ( $\lambda > 400$  nm) from the ground state (Dye) to the triplet excited state (Dye\*). Dye\* excited state species is further transformed into a semi-oxidized radical cation (Dye<sup>+</sup>) by an electron injection into the conduction band of metal oxide. Due to reaction between these trapped electrons and dissolved oxygen in the system, superoxide radical anions ( $O_2^-$ ) are formed which in turn result into hydroxyl radicals ( $OH^-$ ) formation, hence they mainly responsible for the oxidation of the organic compounds. According to many studies, indirect mechanism is generally prevalent over direct mechanism and its contribution to the dye degradation is much more pronounced than the direct mechanism. The latter is believed to be a far slower reaction compared to indirect mechanism<sup>15</sup>. Zirconium dioxide nanoparticles have a wide number of applications owing to non-toxicity, catalytic activity, hydrophilicity, high chemical stability, cost effectiveness<sup>17,19</sup>. It is commonly used in ceramics technology and in heterogeneous catalysis<sup>20</sup>. Due to its property as n-type semiconductor, it has been considered recently as a photocatalyst in photochemical heterogeneous reactions<sup>21</sup>. The relatively wide band gap energy ( $E_g$ ) value (3.25-5.1 eV) and the high negative value of the conduction band potential allowed its use as a photocatalyst in variety of chemical processes such as: the production of hydrogen through water decomposition<sup>20</sup>, oxidation of 2-propanol, propene, carbon monoxide and ethane<sup>23-25</sup> and photodegradation of 4-chlorophenol, 4-nitrophenol and 1,4-pentanediol. It is well known that some dopants involved in a semiconductor matrix, obstruct the recombination of  $e^-/h^+$  pairs and enhance photocatalytic efficiency of the processes<sup>26</sup>. A vast number of techniques have been used to attain metal oxides nanoparticles with variety of sizes, structures and morphologies. Sol-gel is a more convenient technique for synthesize metal oxide nanoparticles which have economic value and large-scale production<sup>27</sup>. Based on these considerations this work aimed to synthesis and characterization of pure  $ZrO_2$ , as well as Fe/ $ZrO_2$  doped samples using Pechini modified Sol-gel method. The aim of the work was extended to include the effect of doping percent on the phase structure, morphological as well as photocatalytic degradation of IC and MB have been investigated.

## Experimental

### Materials and chemicals

Throughout the entire preparation part of the work, double distilled water as well as the following reagent-grade chemicals were used: citric acid,  $ZrOCl_2$ ,  $Fe(NO_3)_3$  (MERCK, Germany);  $(NH_4OH)$  solution (25%). Methylene blue 3,7-Bis(dimethylamino)-phenazo-thionium chloride (Figure 1) was purchased from Aldrich. Indigo Carmine dye was purchased from Fluka.

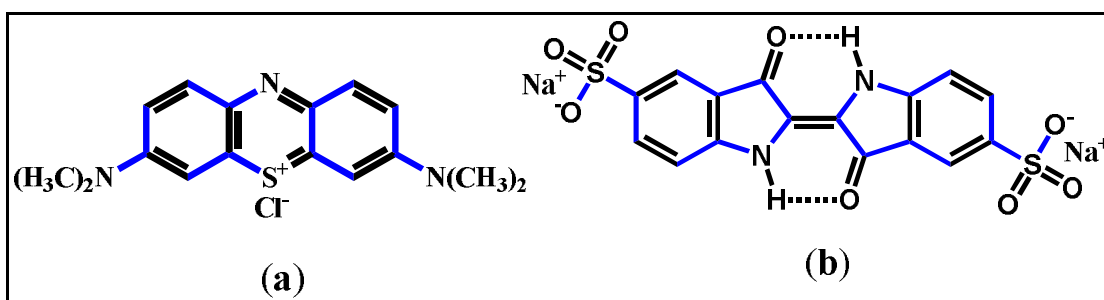


Fig. 1: Chemical structure of a) MB and b) IC

### Characterization methods

The phase composition of samples was determined using XRD in the  $2\theta$  range of  $20-100^\circ$  at room temperature, with a step increase of  $0.02^\circ$  using an XRD diffractometer (X'Pert PRO diffractometer, Cu  $K\alpha$  radiation; PANalytical BV, Almelo, The Netherlands). Based on the XRD patterns, the average crystallite size was determined using the Scherrer's formula<sup>28,29</sup>, and lattice parameters were calculated by the Match software using the Rietveld method<sup>30</sup>. The morphology of the obtained samples was investigated by using scanning electron microscopy and energy-dispersive spectroscopy (EDS) (Ultra Plus; Carl Zeiss Meditec AG, Jena, Germany).

## Photoreactor setup

Photodegradation process investigated in an aqueous medium in order to estimate photocatalytic activity of the prepared naked  $ZrO_2$  as well as the doped  $Fe/ZrO_2$  samples. Photocatalytic degradation experiments were conducted in a borosilicate cylindrical photoreactor with an internal diameter of 4 inch and 5 inch for outer diameter. Hg lamp (500 W) and magnetic stirrer system were fixed in in the photoreactor setup produced from (Eng. Co., Ltd., Egypt). Water cooling circulation system was used to avoid thermal effect could be generated.

## Preparation of $ZrO_2$ and $Fe/ZrO_2$ samples

Preparation of  $ZrO_2$  and  $Fe/ZrO_2$  samples involved mixing of Stoichiometric amount of zirconium/ferric salt with a complexing agent in an aqueous medium. In this study, zirconium oxychloride is used as the zirconium salt whereas ferric nitrate is used as the ferric salt. Citric acid was used as a chelating agent and yields the free impurity oxides. A solution of the ferric nitrate, zirconium oxychloride and Ferric/zirconium salts in the desired (0, 1, 3, 5, 8) mole % were added dropwise to a constantly stirred aqueous solution of the carboxylic acid. Ammonia hydroxide solution was then added drop by drop under continuous stirring. Addition of the diluted basic solution (typically  $NH_4OH$ ) accelerates the hydrolysis process. After then, the pH of the sol is adjusted gradually to 7, which stimulates the gelation process. At this stage a mechanically unstable wet gel is formed. The resulted solution was then vaporized at 70–80 °C under magnetic stirring for about 6h until a xerogel was obtained. The formed xerogel precursor was decomposed at 450 °C for 4 h in air to get rid of the organic substances, and left to cool to room temperature. The decomposed powders were slightly milled using a mortar and calcined in air at 700 °C for 6h and naturally cooled to room temperature.

## Photoactivity measurements

Evaluation of the photocatalytic activity of the nanostructure samples on the photodegradation of dyes was carried out in a liquid–solid phase, in a cylindrical photocatalytic reactor at room temperature. Monitoring of the organic dyes (methylene blue and indigo carmine) degradation was accomplished using a spectrometer (Shimadzu UV 3100, JP). 500 mL aqueous solutions of the dyes, at a previously determined initial concentration, 25 and 50 mg  $L^{-1}$ , for methylene blue and indigo carmine respectively were stocked<sup>31,32</sup>. The slurry containing the desired concentration of the dyes as well as 0.5 g  $L^{-1}$  of the photocatalyst was magnetically stirred throughout the reaction. It was then irradiated with the Hg lamp (500 W) over a period of 180 min. The degradation of the dyes was followed at certain intervals, by drawing an aliquot, filtering through a 0.45  $\mu m$  Millipore filter and recording the diminution of the main absorption bands for each molecule using UV-Vis spectroscopy.

## Results and discussion

### X-ray diffraction

(XRD) The XRD patterns of the free  $ZrO_2$ ,  $Fe_2O_3$  samples as well as the 1-8 % Fe doped samples (FZ1, FZ3, FZ5, FZ8) are shown in Figure 2. The X-ray pattern of undoped  $ZrO_2$  sample goes consistent with the standard pattern of a tetragonal phase of zirconia (JCPDS No 49-1642). The observed diffraction peaks values of 30.30, 34.70, 50.34, and 59.22 originate from the crystal planes (111), (200), (220) and (311). For FZ2 sample, new emerging peaks were observed as weak and broad diffractions at  $\sim$ : 24°, 28.30°, 31.59°, 33°, 41°, 54.5° corresponding to (011), ( $\bar{1}11$ ), (111), (002), (102) and (202) in agreement with a monoclinic phase of zirconia (JCPDS No 88-2390) referring to the presence of two phases of zirconium oxide (monoclinic and cubic) in the FZ1 sample. The intensity of these peaks become more prominent upon raising the doping percent from 1% to 5% suggesting that the Fe-doping process facilitates the transformation of the zirconia from the tetrahedral to monoclinic phase. However, it was surprising observed a complete absence of the two prominent diffraction peaks of the monoclinic phase (at 28.30° and 31.5°) in the diffraction patterns of FZ5 and FZ8 samples presuming that the transformation process was limited by the Fe percent. The absence of these peaks was accompanied by prominent intensifying of (002) diffraction peak and subsequent broadness of the main peak of the zirconia tetragonal phase at 30.30°.

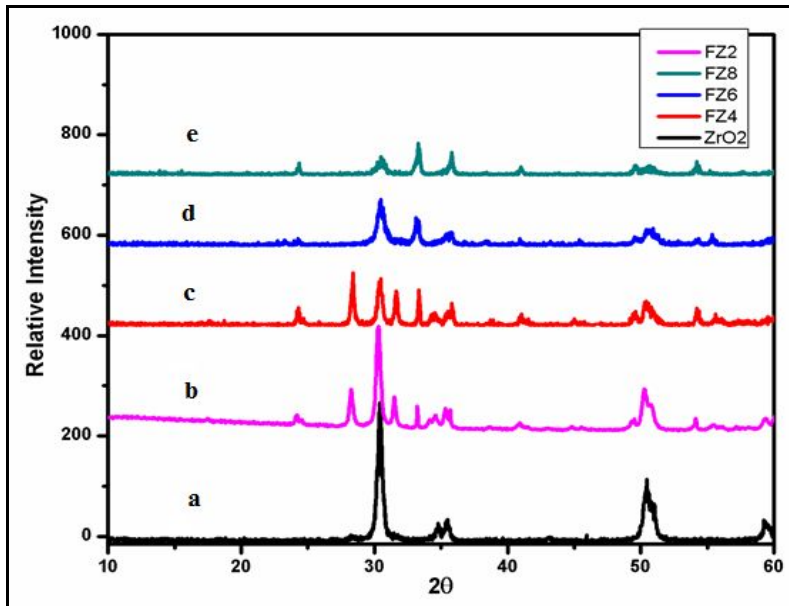


Fig. 2. X-Ray diffraction patterns of a)  $\text{ZrO}_2$  b) 1%Fe/ $\text{ZrO}_2$ , c) 3% Fe/ $\text{ZrO}_2$ , d) 5% Fe/ $\text{ZrO}_2$ , e) 8% Fe/ $\text{ZrO}_2$  nanopowders calcined at 700 °C.

The XRD patterns was used to assess the crystallite size,  $\delta$ , from Scherrer's formula using the most intense diffraction lines.

$$\delta = 0.9\lambda / B \cdot \cos \theta$$

where  $\delta$  is the crystallite size in angstroms ( $\text{\AA}$ ) and corresponds to the diameter of particles,  $\theta$  is the Bragg's angle,  $\lambda$  is the wavelength of the used X-rays, and B is the full-width at half maximum measured in radians of the most intense line in the X-ray powder diffractogram. The calculated average crystallite sizes for each sample are depicted in Table 1. No almost change in size has been noticed between undoped and FZ1. On the other hand, for the other samples, it can be noticed clearly that Fe-doping resulted in reducing the average crystallite size from 30 nm to 18 nm. The lattice parameters (a, b, and c) calculated from these peaks are presented in Table 1. It has been found also that Fe doping resulted in decreasing the lattice parameters (a, b and c) of  $\text{ZrO}_2$  samples, which could be related to the smaller ionic radius of  $\text{Fe}^{3+}$  ( $0.69 \text{ \AA}$ ) relative to  $\text{Zr}^{4+}$  ( $0.86 \text{ \AA}$ ). These findings recorded a similar trend to that formerly reported in the literature<sup>33</sup>.

Table 1: XRD data of Fe/ $\text{ZrO}_2$  samples prepared by sol gel method as function of iron content.

Sample	Direct cell parameters				Crystallite size (nm)
	a( $\text{\AA}$ )	b( $\text{\AA}$ )	c( $\text{\AA}$ )	v( $\text{\AA}$ )	
$\text{ZrO}_2$	5.149 $\text{\AA}$	5.149	5.149	136.5217	29.00
FZ1	5.104	5.104	5.104	132.9852	29.00
FZ3	5.1087	5.1087	5.1087	133.3334	27.05
FZ5	5.1291	5.221	5.0258	134.9346	22.12
FZ8	5.1392	5.1392	5.1392	135.7310	18.26

### Scanning Electron Microscope (SEM)

The aggregation, morphology, and homogeneity of the powders were investigated using SEM technique. The SEM micrographs show similar results for most of the doped samples and some micrographs with different iron content are shown in Figure 3 (a-e). The micrographs of all samples consist of regular nano-sized spherical particles. No prominent change in the morphology parameter was observed by varying the

Fe substitution ratio from 1 to 5%. The micrographs show that the prepared samples composed of relatively uniform and homogeneous spherical particles. Lighter grayish particles (referred to by arrows) was observed distributed over the surface of the zirconia which was assigned to iron oxide nanoparticles. Further, the EDS image (Figure 3c) indicated the presence of Fe adsorbed on the surface of the material.

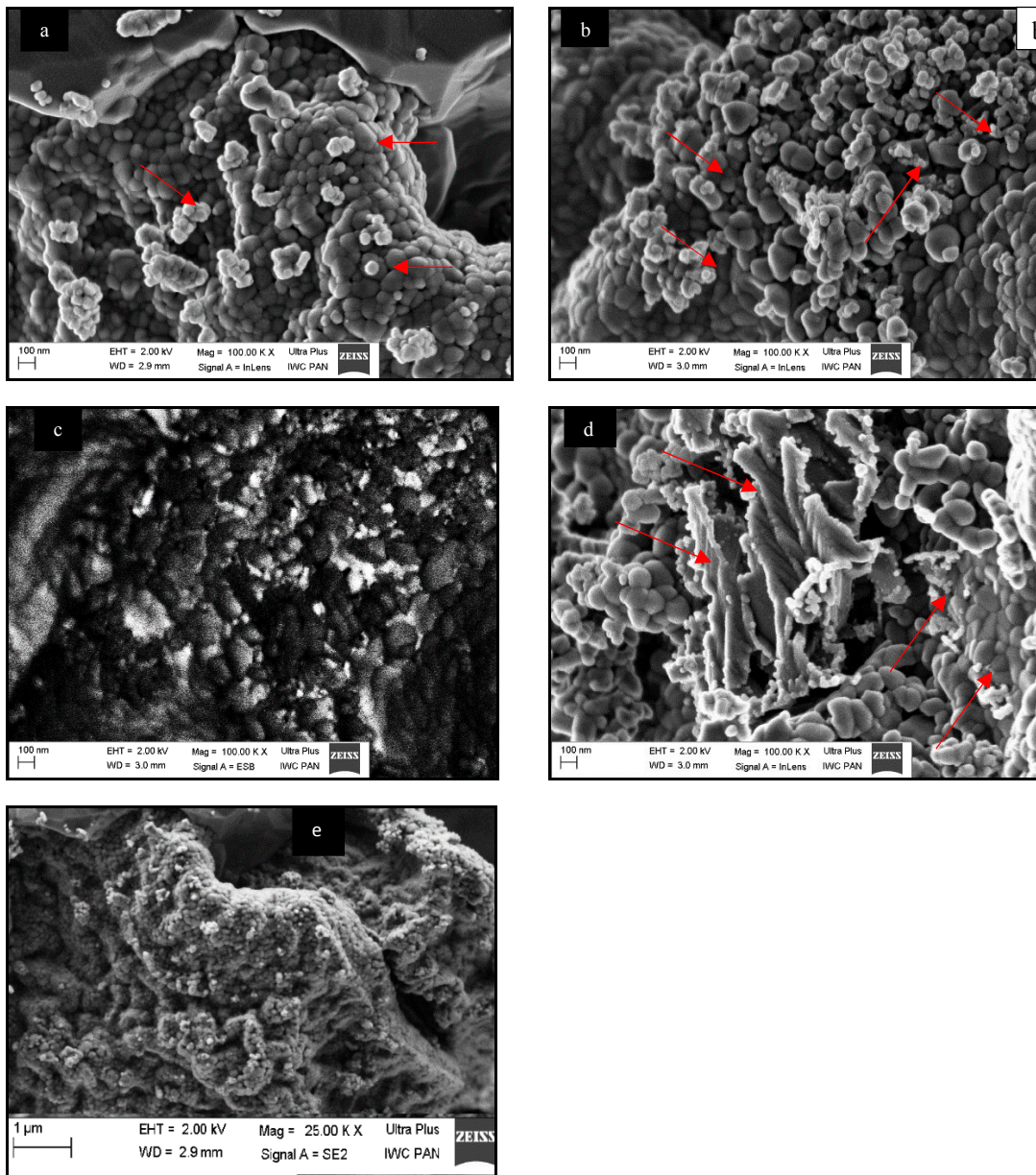


**Fig. 3.** SEM images (a, b, d, e) for (1, 3, 5, 8) % Fe doped  $ZrO_2$  samples, c) EDS image of FZ3.

Heavy elements strongly backscatter electrons, hence those areas appear brighter while the lighter elements tend to absorb electrons and thus appear darker<sup>34</sup>. The EDS image (Figure 3c) confirmed the presence of Fe as shown as brighter particles and Zr as shown in a darker color.

### Photocatalytic degradation of MB and IC

The synthesized samples showed color gradation from white for the undoped  $ZrO_2$  sample to light brown upon increasing the Fe content (Figure 4). This change in color can be attributed to an increase in visible light absorption upon increasing of the  $Fe^{3+}$  dopant content. Absorption of visible light can be assigned to generation of new  $Fe^{3+}/Fe^{4+}$  dopant energy level within the band gap of  $ZrO_2$ , electronic d–d transition and/or charge transfer (CT) transition between the  $Fe^{3+}$  ions<sup>35</sup>.

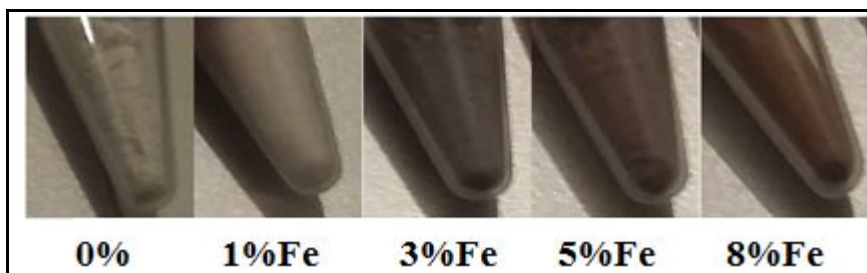


**Fig. 4. Color gradation of undoped  $ZrO_2$  and doped  $Fe/ZrO_2$  nanocomposites (1 -8 % Fe)**

Photodegradation process of methylene blue and indigo carmine on the zirconia matrix could be assigned to absorption of light with sufficient energy for band gap excitation, which results in excitation of an electron ( $e^-$ ) from the valance band (leaving a hole) to the conduction band. On the surface of  $ZrO_2$ , these photogenerated holes transfer charge with the surface-bound organic dyes which is then subjected to undergo oxidative reactions by either indirect via hydroxyl-like pathways or direct electron transfer from the organic dye to photogenerated hole or another photogenerated reactive species, like  $HO^\bullet$ <sup>36</sup>. A significant influence of the iron loading on photocatalytic activity of Fe-Zr samples was observed. It was observed that the degradation of the dye increases gradually as the iron dopant percent increased. This could be assigned to that introducing of  $Fe^{3+}$  ions into  $ZrO_2$  matrix, leads to enhancement in absorption of light, extending the spectral response of photocatalyst to longer wavelength and hence lowering the band gap energy in pristine zirconia<sup>37</sup>.

The photodegradation percentages calculated by measuring the relative decrease in the methylene blue and indigo carmine dyes concentration upon Fe-doping against the initial value at different irradiation times were illustrates Figure 5. Both of the dyes showed similar degradation behavior. As it was found that the degradation percentage increase upon increasing the iron doping percent. It can be observed that all the nanocomposites recorded higher photodegradation ability than the naked  $ZrO_2$ . These outcomes refer that the Fe doping noticeably improved the dye degradation, as Fe-doping changes chemistry of the zirconia surface and produce changes in the electronic its structure. In the beginning of photocatalytic degradation process, it was observed that the photodegradation percentage were in the ranges (6-11 %) and (4-10 %) at zero irradiation time for methylene blue and indigo carmine dyes respectively. After 15 min of irradiation, the degradation percentages markedly raised to be in the ranges (37-48%) and (33-43 %) for MB and IC respectively. At all-time intervals FZ8 sample recorded the highest degradation percentage. As it was found to be 74, 88 and 94 % for MB and 58, 80 and 88 % for IC after time interval of 60, 120 and 180 minutes respectively in Figure 5. The catalytic activity of several nanostructures of  $\alpha-Fe_2O_3$  nanoparticles reported in the literature recorded values that are inferior to the values attained in this study<sup>27</sup>. It is worth noticing also that the photodegradation ability of a catalytic material is influenced by its crystallite size, decreasing the crystallite size upon raising the doping percent has a positive impact on photocatalytic activity of the zirconium doped catalysts (Table 2). The presence of smaller crystallite sized provided more active sites along the surface of the catalyst and hence enhancing the photodegradation ability.

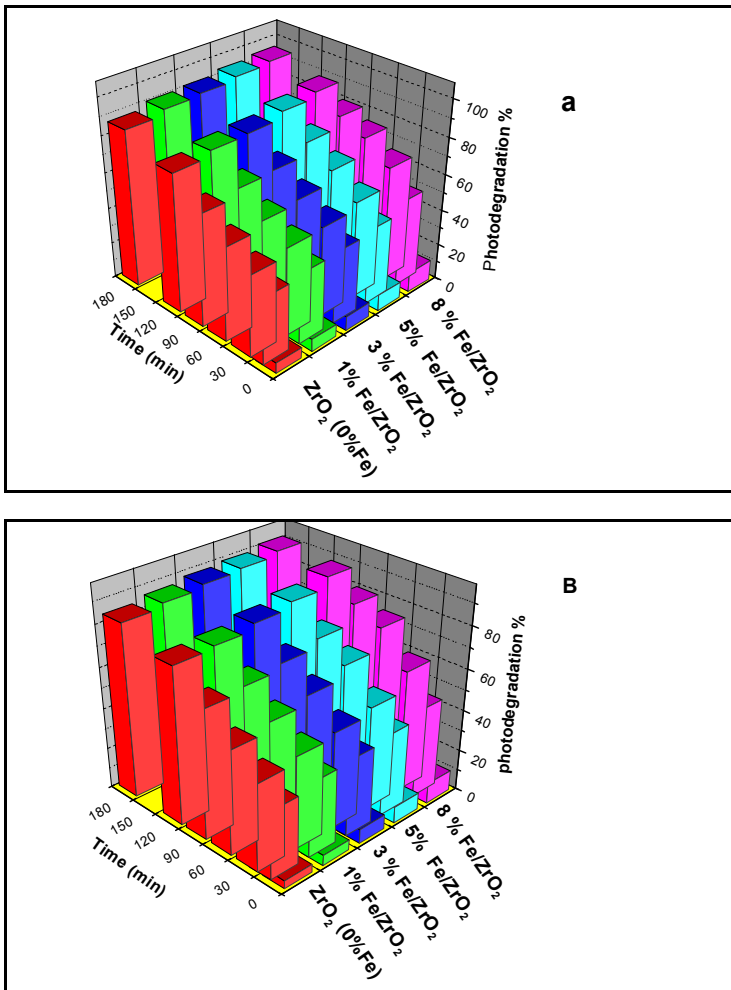


**Fig. 5. Correlation between photodegradation process percentage of a) MB and b) IC with different Fe content at different intervals time.**

The efficiency of iron percent on the photodegradation of the dyes is more clear by plotting the photodegradation percentages efficiency for the various samples at a certain time of 60 min (Figure 6), it was observed that changing the iron percent were highly effective on photocatalytic degradation percentages the samples

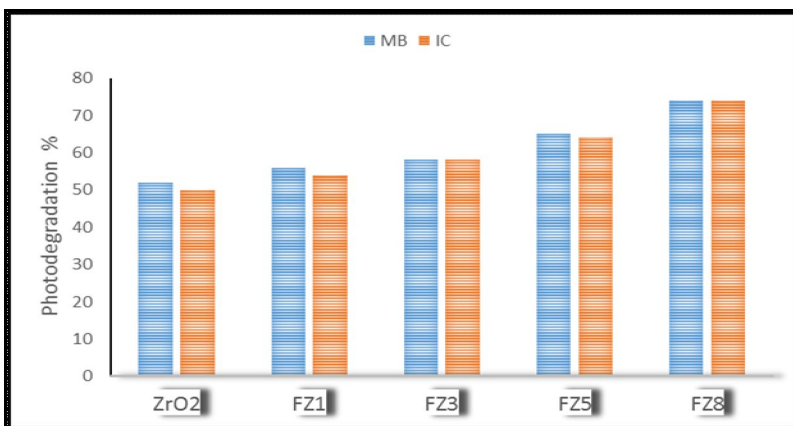


**Fig. 6. Comparison of photodegradation process percentage of MB and IC with different Fe content at 60 min.**

Figure 7 (a, b) shows that photocatalytic degradation rates of MB and IC fits into first order kinetics under the used simulated solar irradiation system. Photocatalytic degradation rates of MB and IC listed in table 2, increases with the iron loading from 1 to 8%. This could be attributed to the interaction between the doping metal centers and zirconium oxide support. Such interaction could be explained by the dual  $Zr^{4+}$  role, as a hole and electron trap and as electron-hole pair recombination center<sup>38</sup>. The incorporation of iron dopant results in modifying the structure as well as raising number of defects within the framework of zirconia and increasing the photoactivity of the oxide. They may also inhibit the recombination of photo electron and hole pairs induced by the zirconia matrix. Moreover, it is worth noticing that decreasing the crystallite size upon raising the doping percent has a positive impact on photocatalytic activity of the zirconium doped catalysts (Table 2).

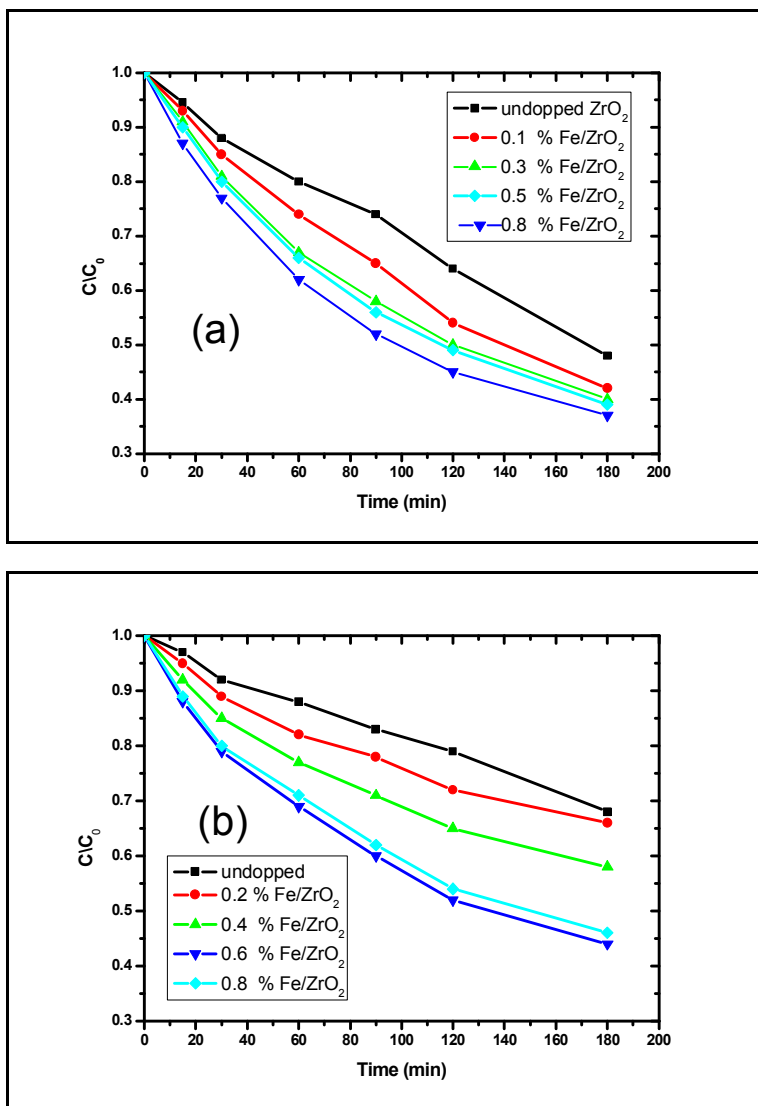


**Figure 7: Photocatalytic degradation rates of (a) MB and (b) IC with different Fe content**

The natural logarithm of the variation in the relative concentrations of MB and IC as a function of irradiation time are shown in Figure 8 (a, b), respectively. The kinetics of the degradation reaction can be described using a first-order model. The pseudo first-order kinetics equation is expressed as

$$\ln(C_0/C_t) = k_{app} t$$

where  $C_t$  is the dye concentration in aqueous solution at time  $t$  ( $mg L^{-1}$ ),  $C_0$  is the initial dye concentration ( $mg L^{-1}$ ), and  $k_{app}$  is the apparent pseudo-first-order kinetic constant ( $min^{-1}$ ). The values of  $k_{app}$  are listed in table 2. The excellent fitting indicates that the photodegradation processes follows first-order reaction kinetics. It is

noteworthy that the photocatalytic degradation of MB on the tested samples recorded higher rate values than that of IC (Table 2).

**Table (2): Photocatalytic degradation rates ( $\text{min}^{-1}$ ) of MB and IC**

Sample	MB	IC
ZrO <sub>2</sub>	0.3950	0.3064
FZ1	0.4202	0.3242
FZ3	0.4246	0.3301
FZ5	0.4256	0.3314
FZ8	0.4295	0.3320

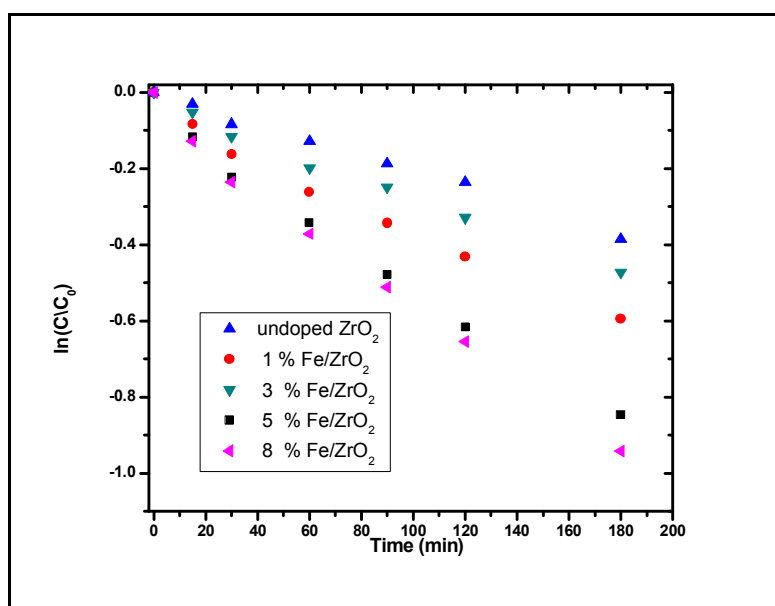
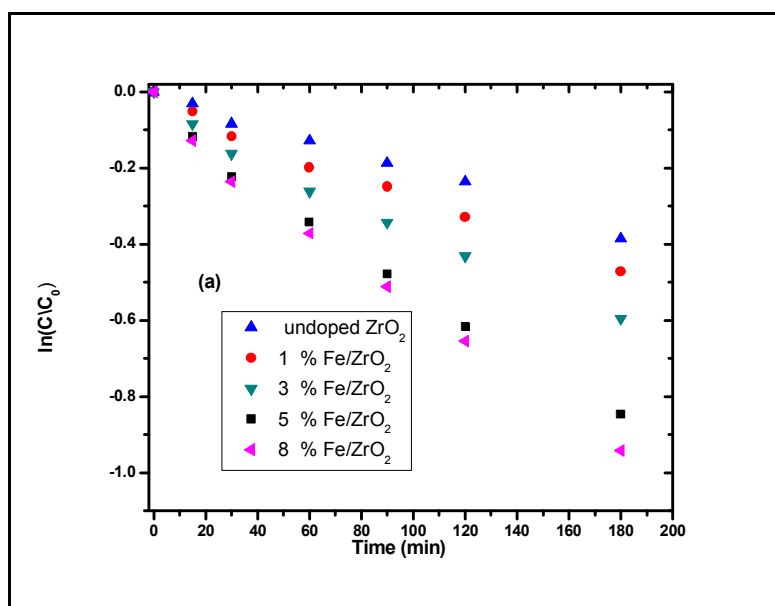


**Fig. 8: linear plots of a) methylene blue and b) Indigo carmine plotted as  $\ln(Co/Ct)$  versus time at different Fe content**

## Conclusion

Sol gel modified Pechini method was used to prepare pure  $ZrO_2$  as well as doped Fe/ $ZrO_2$  oxide with varying iron content (1, 3, 5 and 8 mole percent %). The synthesized samples present phases varied between tetragonal and monoclinic  $ZrO_2$  upon varying the doping percent. The average crystallite size varied between 30 nm for the unpoed samples to 18 nm for the 8% Fe/ $ZrO_2$ . All samples consist of regular nano-sized spherical particles. Compared to the pure oxide, all iron dopant percents resulted in enhancement of the methylene blue and indigo carmine photodegradation reaction rates, showing that the Fe ions incorporation to the  $ZrO_2$  lattice improves its photocatalytic activity. It is worth noticing that decreasing the crystallite size upon raising the doping percent has a positive impact on photocatalytic activity of the zirconium doped catalysts. At all-time intervals FZ8 sample recorded the highest degradation percentage. The photodegradation processes follows first-order reaction kinetics. The photocatalytic degradation of MB on the tested samples recorded higher rate values than that of IC. The superior photocatalytic performance of the synthesized Fe/ $ZrO_2$  nanocomposites can be extended to study their ability to remove other organic pollutants from waste water.

## References

1. Chatterjee A, Das D, Chakraborti D., A study of ground water contamination by arsenic in the residential area of Behala, Calcutta due to industrial pollution. *Environmental Pollution*, 1993, 80: 57-65.
2. Corn M, Handbook of hazardous materials, Academic Press, 2012.
3. Gautam R K, Rawat V, Banerjee S, Sanroman M A, Soni S, Singh S K, Chattopadhyaya M C., Synthesis of bimetallic Fe-Zn nanoparticles and its application towards adsorptive removal of carcinogenic dye malachite green and Congo red in water. *Journal of Molecular Liquids*, 2015, 212: 227-236.
4. Fu J, Xin Q, Wu X, Chen Z, Yan Y, Liu S, Wang M, Xu Q, Selective adsorption and separation of organic dyes from aqueous solution on polydopamine microspheres. *Journal of Colloid and Interface Science*, 2016, 461: 292-304.
5. Hazzaa R, Hussein M, Adsorption of cationic dye from aqueous solution onto activated carbon prepared from olive stones. *Environmental Technology & Innovation*, 2015, 4: 36-51.
6. Cao Y, Gu X, Yu H, Zeng W, Liu X, Jiang S, Li Y, Degradation of organic dyes by Si/SiO<sub>x</sub> core-shell nanowires: Spontaneous generation of superoxides without light irradiation. *Chemosphere*, 2016, 144: 836-841.
7. Karnjkar Y S, Dinde R M, Dinde N M, Bawankar K N, Hinge S P, Mohod A V, Gogate P R, Degradation of magenta dye using different approaches based on ultrasonic and ultraviolet irradiations: Comparison of effectiveness and effect of additives for intensification. *Ultrasonics Sonochemistry*, 2015, 27: 117-124.
8. Bansal P, Chaudhary G R, Mehta S K, Comparative study of catalytic activity of  $ZrO_2$  nanoparticles for sonocatalytic and photocatalytic degradation of cationic and anionic dyes. *Chemical Engineering Journal*, 2015, 280: 475-485.
9. Khunrattanaphon P., Chavadej S., Sreethawong T., Synthesis and application of novel mesoporous-assembled  $SrTi_xZr_{1-x}O_3$ -based nanocrystal photocatalysts for azo dye degradation. *Chemical Engineering Journal*, 2011, 170: 292-307.
10. Ljubas D, Smoljanić G, Juretić H, Degradation of Methyl Orange and Congo Red dyes by using  $TiO_2$  nanoparticles activated by the solar and the solar-like radiation. *Journal of Environmental Management*, 2015, 161: 83-91.
11. EL-Mekki M, Nady N, Abdelwahab N A, Mohamed Walied A A and Abdel-Mottaleb M S A, Flexible Bench-Scale Recirculating Flow CPC Photoreactor for Solar Photocatalytic Degradation of Methylene Blue Using Removable  $TiO_2$  Immobilized on PET Sheets. *International Journal of Photoenergy*, Doi.10.1155/2016/9270492, 2016, Article ID 9270492, 9 pages
12. Ajmal A, Majeed I, Malik R N, Idriss H, Nadeem M A, Principles and mechanisms of photocatalytic dye degradation on  $TiO_2$  based photocatalysts: a comparative overview. *Rsc Advances*, 2014, 4: 37003-37026.

13. Hernández A, Maya L, Sánchez-Mora E, Sánchez E M, Sol-gel synthesis, characterization and photocatalytic activity of mixed oxide ZnO-Fe<sub>2</sub>O<sub>3</sub>. *Journal of sol-gel science and technology*, 2007, 42: 71-78.
14. EL-Mekki D M, Galal H R, Abd EL Wahab R M., Mohamed Walied A A, Photocatalytic activity evaluation of TiO<sub>2</sub> nanoparticles based on COD analyses for water treatment applications: a standardization attempt. *Int. J. Environ. Sci. Technol.*, 2016, DOI 10.1007/s13762-016-0944-0, 12 pages.
15. Grätzel M, *Photoelectrochemical cells*. *Nature*, 2001, 414: 338-344.
16. Adhikari S, Sarkar D, Metal oxide semiconductors for dye degradation. *Materials Research Bulletin*, 2015, 72: 220-228.
17. M. Hoffmann, Martin ST, Choi W and Bahnemann DW, *Chem. Rev*, 1995, 95: 69.
18. Daneshvar N, Rasoulifard M, Khataee A, Hosseinzadeh F, Removal of CI Acid Orange 7 from aqueous solution by UV irradiation in the presence of ZnO nanopowder. *Journal of Hazardous Materials*, 2007, 143: 95-101.
19. Manoharan D, Loganathan A, Kurapati V, Nesamony V J, Unique sharp photoluminescence of size-controlled sonochemically synthesized zirconia nanoparticles. *Ultrasonics Sonochemistry*, 2015, 23: 174-184.
20. Bansal P, Chaudhary G R, Mehta S, Comparative study of catalytic activity of ZrO<sub>2</sub> nanoparticles for sonocatalytic and photocatalytic degradation of cationic and anionic dyes. *Chemical Engineering Journal*, 2015, 280: 475-485.
21. Li L, Cheng L, Fan S, Gao X, Xie Y, Zhang L, Fabrication and dynamic compressive response of laminated ZrO<sub>2</sub>-Zr<sub>2</sub>CN/Si<sub>3</sub>N<sub>4</sub> ceramics. *Ceramics International*, 2015, 41: 8584-8591.
22. Kim J Y, Kim C S, Chang H K, Kim T O, Synthesis and characterization of N-doped TiO<sub>2</sub>/ZrO<sub>2</sub> visible light photocatalysts. *Advanced Powder Technology*, 2011, 22: 443-448.
23. Biswas P, Kunzru D, Steam reforming of ethanol for production of hydrogen over Ni/CeO<sub>2</sub>-ZrO<sub>2</sub> catalyst: effect of support and metal loading. *International Journal of Hydrogen Energy*, 2007, 32: 969-980.
24. Labaki M, Siffert S, Lamonier J F, Zhilinskaya E A, Aboukais A, Total oxidation of propene and toluene in the presence of zirconia doped by copper and yttrium: role of anionic vacancies. *Applied Catalysis B: Environmental*, 2003, 43: 261-271.
25. Wootsch A, Descorme C, Duprez D, Preferential oxidation of carbon monoxide in the presence of hydrogen (PROX) over ceria-zirconia and alumina-supported Pt catalysts, *Journal of Catalysis*, 2004, 225: 259-266.
26. Wang S, Murata K, Hayakawa T, Hamakawa S, Suzuki K, Excellent performance of lithium doped sulfated zirconia in oxidative dehydrogenation of ethane. *Chemical Communications*, 1999, 103-104.
27. Lopez T, Alvarez M, Tzompantzi F, Picquart M, Photocatalytic degradation of 2, 4-dichlorophenoxyacetic acid and 2, 4, 6-trichlorophenol with ZrO<sub>2</sub> and Mn/ZrO<sub>2</sub> sol-gel materials. *Journal of sol-gel science and technology*, 2006, 37: 207-211.
28. Fouda M F R, ElKholi M B, Mostafa S A, Hussien A I, Wahba M A, El-Shahat M F, Characterization and evaluation of nano-sized α Fe<sub>2</sub>O<sub>3</sub> pigments synthesized using three different carboxylic acid. *Adv. Mat. Lett.*, 2013, 4: 347-353.
29. Patterson AL, The Scherrer formula for X-ray particle size determination. *Physical review*, 1939, 56: 978.
30. Scherrer P, *Göttinger Nachrichten Gesell.*, Search PubMed, 1918, 2: 98.
31. Young R, Introduction to the Rietveld method. *The Rietveld Method*, 1993, 5: 1-38.
32. Hanna Adli A, Mohamed Walied A A, Ibrahim I A, Studies on photodegradation of Methylene Blue (MB) by nano-sized titanium oxide, *Egyptian journal of chemistry*, 2014, 57: 315-326.
33. El-sayed Badr A., Ibrahim I A, Mohamed Walied A A, Ahmed M A M, Synthesis and Characterization of Crystalline Nano TiO<sub>2</sub> and ZnO and their effects on the photodegradation of Indigo Carmine dye. *International Journal of Advanced Engineering and Nano Technology*, 2015, 2, 12: 15-22.
34. Qadri S B, Kim H, Horwitz J, Chrisey D, Transparent conducting films of ZnO-ZrO<sub>2</sub>: Structure and properties. *Journal of Applied Physics*, 2000, 88: 6564-6566.
35. Krinsley D H, Pye K, Boggs Jr S, Tovey N K, Backscattered scanning electron microscopy and image analysis of sediments and sedimentary rocks. Cambridge University Press, 2005.

37. Sood S, Umar A, Mehta S K, Kansal S K, Highly effective Fe-doped TiO<sub>2</sub> nanoparticles photocatalysts for visible-light driven photocatalytic degradation of toxic organic compounds. *Journal of Colloid and Interface Science*,2015,450: 213-223.
38. Hoffmann M R, Martin S T, Choi W, Bahnemann D W, Environmental applications of semiconductor photocatalysis. *Chemical reviews*, 1995, 95: 69-96.
39. Araña J, González Díaz O, Miranda Saracho M, Doña Rodríguez J M, Herrera Melián J A, Pérez Peña J, Photocatalytic degradation of formic acid using Fe/TiO<sub>2</sub> catalysts: the role of Fe<sup>3+</sup>/Fe<sup>2+</sup> ions in the degradation mechanism. *Applied Catalysis B: Environmental*, 2001, 32: 49-61.
40. Zhu J, Zheng W, He B, Zhang J, Anpo M, Characterization of Fe–TiO<sub>2</sub> photocatalysts synthesized by hydrothermal method and their photocatalytic reactivity for photodegradation of XRG dye diluted in water. *Journal of Molecular Catalysis A: Chemical*, 2004, 216: 35-43.

\*\*\*\*\*